$[Fe(OEP^{\bullet})(X)]^{+}$ π-Cation Radicals: Characterization and Spin−Spin Interactions

Charles E. Schulz,*,† Hungsun Song,‡ Anil Mislankar,‡ Robert D. Orosz,§ Christopher A. Reed,*,§ Peter G. Debrunner,*,|| and W. Robert Scheidt*,‡

Departments of Physics, Knox College, Galesburg, Illinois 61401, and University of Illinois, Urbana, Illinois 61801, Department of Chemistry and Biochemistry, University of Notre Dame, Notre Dame, Indiana 46556, and Department of Chemistry, University of Southern California, Los Angeles, California 90089-0744

Received August 28, 1996[⊗]

The preparation and characterization of the π-cation radical derivatives of [Fe(OEP)(X)] (X = Cl^-, Br^-) is reported. Three different derivatives have been prepared: $[Fe(OEP^{\bullet})(Cl)]ClO_4$, $[Fe(OEP^{\bullet})(Cl)][SbCl_6]$, and $[Fe(OEP^{\bullet})(Br)][SbCl_6]$. All derivatives have been characterized by UV−vis, IR, and Mössbauer spectroscopy. In addition, $[Fe(OEP^{\bullet})(Cl)]ClO_4$ has been characterized by a single-crystal structure determination, and $[Fe(OEP^{\bullet})(Cl)][SbCl_6]$ and [Fe(OEP)(Br)][$SbCl_6$] have been studied by temperature-dependent magnetic susceptibility measurements and Mössbauer measurements in an applied magnetic field. The X-ray structure of $[Fe(OEP^{\bullet})(Cl)]ClO_4$ reveals a five-coordinate porphyrinate species that forms tight cofacial $\pi-\pi$ dimers in which the two porphyrin rings are almost exactly overlapped with an inter-ring separation of 3.24 Å, a lateral shift of 0.2 Å, and a twist angle between the two rings of 31.2°; the two iron atoms are 4.112 Å apart. Crystal data: $C_{37}H_{46}FeCl_4O_4N_4$, a = 27.454(7) Å, b = 15.322(3) Å, c = 19.802(3) Å, β = 116.14 (2)°, monoclinic, $C2/c$, Z = 8. Iron(III) is found to be in the high-spin state in all derivatives. The magnetic data (susceptibility and Mössbauer) have been interpreted in terms of two spin coupling models. Both models give a picture of strong coupling between the various spins in the dimeric species. In the model judged to best fit all data with a physically meaningful zero-field splitting, there are three terms in the total Hamiltonian: an axial zero-field splitting parameter D for the high-spin iron, an intramolecular antiferromagnetic coupling $-2J_{Fe-r}(\vec{S}\cdot\vec{s})$ between the iron spin $S = {}^5/_2$ and the π-cation radical $s = {}^1/_2$ spin, and an intermolecular antiferromagnetic coupling $-2J_{R-R}(\vec{S}+\vec{s})\cdot(\vec{S}'+\vec{s}')$ between the total spins on each half of the dimer.

Introduction

In earlier work on metalloporphyrin π-cation radicals,[1−6] we have investigated the variety of spin couplings between the metal ion and porphyrin ring in a number of derivatives that differ in metal ion, axial ligation, and/or porphyrin ligand. Both intra- and intermolecular spin coupling can be significant.[7] Two distinct *intra*molecular coupling mechanisms are found: (i) ferromagnetic coupling between the metal and ligand magnetic centers, leading to maximal spin multiplicity and (ii) antiferromagnetic coupling, effectively leading to a lower multiplicity state. It is found that case i is observed when the porphyrin ring is essentially planar and approximates D_{4h} symmetry. In this symmetry, the partially filled metal orbitals and the porphyrin π-radical orbital are orthogonal, which then leads to Hund's rule-like maximum spin multiplicity. Case ii arises in lower symmetry systems where the metal and ligand magnetic orbitals are not strictly forbidden by symmetry from net overlap. The copper(II) π-cation radicals of TPP[2,8] and TMP,[4] which are $S = 0$ and $S = 1$ species, respectively, nicely illustrate these important core conformation effects on magnetic coupling. Fajer and co-workers[9] have recently confirmed the effects of core ruffling with the use of a sterically congested copper(II) radical π-cation complex; the compound is diamagnetic, as expected for this severely ruffled derivative. In well-characterized systems that display *inter*molecular coupling, it is the unpaired electrons on the porphyrin rings that are coupled. The magnitude of the coupling ranges from $2J = -14.7$ cm^{-1} in one crystalline form of weakly coupled $[Zn(TPP^{\bullet})(OClO_3)]$ dimers to greater than -200 cm^{-1} in the strongly coupled (diamagnetic) dimer $[Zn(OEP^{\bullet})(OH_2)]_2(ClO_4)_2$.[4]

Cases where both intra- and intermolecular spin coupling can be significant are less well understood. The $[Cu(OEP^{\bullet})]^+$ and $[Cu(OEC^{\bullet})]^+$ radical systems exhibit Cu−Cu triplet EPR spectra[10] with no evidence for unpaired radical electrons in either the EPR[10] or the bulk magnetic susceptibility.[11] The results are consistent with pairwise interacting complexes. It is presumed that these copper species have strongly overlapped, cofacial ring pairs like those found in the zinc and nickel

† Know College.
‡ University of Notre Dame.
§ University of Southern California.
|| University of Illinois.
⊗ Abstract published in *Advance ACS Abstracts,* January 15, 1997.

(1) Gans, P.; Buisson, G.; Duée, E.; Marchon, J.-C.; Erler, B. S.; Scholz, W. F.; Reed, C. A. *J. Am. Chem. Soc*. **1986**, *108*, 1223.
(2) Erler, B. S.; Scholz, W. F.; Lee, Y. J.; Scheidt, W. R.; Reed, C. A. *J. Am. Chem. Soc*. **1987**, *109*, 2644.
(3) Song, H.; Rath, N. P.; Reed, C. A.; Scheidt, W. R. *Inorg. Chem*. **1989**, *28*, 1839.
(4) Song, H.; Reed, C. A.; Scheidt, W. R. *J. Am. Chem. Soc*. **1989**, *111*, 6865.
(5) (a) Song, H.; Reed, C. A.; Scheidt, W. R. *J. Am. Chem. Soc*. **1989**, *111*, 6867. (b) Song, H.; Orosz, R. D.; Reed, C. A.; Scheidt, W. R. *Inorg. Chem*. **1990**, *29*, 4274.
(6) Schulz, C. E.; Song, H.; Lee, J. Y.; Mondal, J. U.; Mohanrao, K.; Reed, C. A.; Walker, F. A.; Scheidt, W. R. *J. Am. Chem. Soc*. **1994**, *116*, 7196.
(7) Reed, C. A.; Orosz, R. D. In *Research Frontiers in Magnetochemistry*; O'Connor, C. J., Ed.; World Scientific: Singapore, 1993; pp 351−393.
(8) Abbreviations used: TMP, dianion of tetramesitylporphyrin; TPP, dianion of tetraphenylporphyrin; OEP, dianion of octaethylporphyrin; OEC, dianion of octaethylchlorin; a raised dot in the formula of the porphyrin indicates a π-cation radical, e.g., $OEP^{\bullet}$ for the OEP π-cation radical.
(9) Renner, M. W.; Barkigia, K. M.; Zhang, Y.; Medforth, C. J.; Smith, K. M.; Fajer, J. *J. Am. Chem. Soc*. **1994**, *116*, 8582.
(10) Mengerson, C.; Subramanian, J.; Fuhrhop, J.-H. *Mol. Phys*. **1976**, *32*, 1299.

S0020-1669(96)01053-1 CCC: $14.00

complexes[5] and in related examples of other [M(OEP•)] π-cation radicals.[12] In the six-coordinate complex [VO(OH$_2$)(OEP•)]-SbCl$_6$,[6] where the two axial ligands inhibit the face to face approach of the two porphyrin rings, there is only a "saw-toothed" edge to edge contact between the two radical rings. Nonetheless, the most satisfactory model that explains the physical data is one with intramolecular ferromagnetic coupling (between the metal and radical) and fairly strong antiferromagnetic intermolecular coupling ($2J_{r-r} = -139$ cm^{-1}) between two radical spins, rather than just simple mononuclear, intramolecular coupling.

In an earlier communication,[14] we reported the molecular structure, magnetic susceptibility, and Mössbauer spectra of the π-cation radical derivative of chloro(octaethylporphinato)iron-(III), [Fe(OEP•)(Cl)]$^+$. Two distinct models with different intermolecular coupling constants were found to provide adequate fits of the Mössbauer and magnetic susceptibility data; both are fully consistent with high-spin iron(III) species. To confirm the applicability of these models, we have now characterized a related bromo derivative, [Fe(OEP•)(Br)]$^+$, as its hexachloroantimonate salt. We also fully report on our characterization of the chloro derivative [Fe(OEP•)(Cl)]$^+$ and the further development of models for the magnetic interactions.

Experimental Section

General Information. UV−vis spectra were recorded on Perkin-Elmer Lambda 6 and 19 spectrophotometers and IR spectra on a Perkin-Elmer 883 spectrometer. EPR spectra were measured on a Varian E-Line spectrometer operating at X-band frequency. Mössbauer spectra were measured on ground crystals as Apiezon grease suspensions at 4.2 and 200 K in a zero field and with a 4.5 T applied magnetic field at a number of temperatures. All solid-state samples for the spectroscopy measurements were prepared in a Vacuum Atmospheres drybox. All reactions were performed under an argon atmosphere with Schlenkware and cannula techniques. Dichloromethane was dried by distillation from CaH_2, and pentane and hexanes were dried by distillation from sodium−benzophenone. Tris(*p*-bromophenyl)aminium hexachloroantimonate was purchased from Aldrich. Iron was inserted into H_2OEP by standard techniques.[15] Thianthrenium perchlorate was prepared by literature procedures.[16] *Caution*: These perchlorate-containing materials can detonate spontaneously and should be handled only in small quantities; other safety precautions are also warranted. We have experienced an explosion of thianthrenium perchlorate under mild heating but have had no difficulties with the porphyrin radical salts.[17]

Preparation of [Fe(OEP•)(Cl)]ClO$_4$. [Fe(OEP)(Cl)] (51.3 mg, 0.0822 mmol) and thianthrenium perchlorate (25.4 mg, 0.0804 mmol) were placed in a 100 mL Schlenk flask, and dichloromethane (∼15 mL) was added. The solution was stirred for 10 min, filtered, and transferred into 10 mL beakers, which were placed in crystallizing bottles under argon for crystallization. One crystallizing bottle contained hexanes as the nonsolvent and the other one had pentane. Both bottles were placed in a refrigerator (4 °C) for crystallization. Two days later, both bottles were opened and the crystals were harvested. A suitable crystal for X-ray diffraction study was obtained from the crystallization with pentane as the nonsolvent. These crystallization experiments always resulted in the formation of both [Fe(OEP•)(Cl)]ClO$_4$ and [Fe(OEP•)(OClO$_3$)$_2$]. The two products could be differentiated by the morphology of the crystals. In our experiments, crystals of [Fe(OEP•)(Cl)]ClO$_4$ have hexagonal shapes while those of [Fe(OEP•)(OClO$_3$)$_2$] have parallelepiped shapes. UV−vis and IR spectra were measured on samples comprised of selected crystals. UV−vis (CH_2Cl_2 solution): λ_{max} 356 (Soret), 518, 581 nm. IR (KBr): ν(OEP•) 1533 cm^{-1} (broad); ν(ClO$_4$) 1144 (strong, broad), 623 cm^{-1}; ν(Fe−Cl) 353 cm^{-1} (broad).

Bulk samples were prepared by the following procedure: [Fe(OEP)-(Cl)] (97.5 mg, 0.156 mmol) and thianthrenium perchlorate (49.2 mg, 0.156 mmol) were dissolved in dichloromethane in a 100 mL Schlenk flask. The solution was placed in a sonicator for 1 min and then filtered into pentane. The resulting precipitate was filtered and washed with pentane until the filtrate was colorless. The product was dried under vacuum (yield 75%).

Preparation of [Fe(OEP•)(Cl)][SbCl$_6$]. [Fe(OEP)(Cl)] (89.7 mg, 0.144 mmol) and tris(*p*-bromophenyl)aminium hexachloroantimonate (115.9 mg, 0.142 mmol) were dissolved in dichloromethane (∼15 mL) in a 100 mL Schlenk flask. The solution was stirred for an hour, and the solvent was removed under vacuum until ∼5 mL of solvent remained. The solution was filtered, and the product was washed with a small amount of dichloromethane (yield 92%). UV−vis (CH_2Cl_2 solution): λ_{max} 356 (Soret), 518, 576 nm. IR (KBr): ν(OEP•) 1532 cm^{-1} (strong); ν(SbCl$_6$) 344 cm^{-1} (strong).

Preparation of [Fe(OEP•)(Br)]SbCl$_6$. [Fe(OEP)(Br)] (200 mg, 0.299 mmol) and tri-(*p*-bromophenyl)aminium hexachloroantimonate (248 mg, 0.304 mmol) were placed in a Schlenk flask and degassed for 1 h. About 20 mL of dichloromethane was then introduced into the flask through a cannula under argon. Immediately a brown-colored precipitate began to appear. The mixture was stirred for 1.5 h. The solution was filtered, and the product was washed with dichloromethane to remove unreacted [Fe(OEP)(Br)] and NR_3 SbCl$_6$. The product was then dried under vacuum (yield 90%). UV−vis (CH_2Cl_2 solution): λ_{max} 358 (Soret), 519, 586, 623 nm. IR (KBr): ν(OEP•) 1535 cm^{-1} (strong); ν(SbCl$_6$) 344 cm^{-1}.

Magnetic Susceptibility Measurements. Measurements were performed on lightly compressed samples (∼30 mg) in an aluminum bucket on a SHE Model 905 SQUID susceptometer at 2 and 10 kG. When samples were ground vigorously, as is usual for magnetic susceptibility measurements, inconsistent data were obtained. An apparent lattice disruption occurred, and these data were not used.

X-ray Diffraction Studies. A suitable dark-brown single crystal of [Fe(OEP•)(Cl)]ClO$_4$·CH$_2$Cl$_2$, with approximate dimensions 0.07 × 0.27 × 0.31 mm, was subjected to preliminary examination at 123 ± 2 K. An Enraf-Nonius CAD4 diffractometer equipped with a locally modified Syntex LT-1 cooling system and with graphite-monochromated Mo Kα radiation (λ = 0.710 73 Å) was used. Final cell constants and space group are reported in Table 1. The choice of the centrosymmetric space group was supported by the E-statistics and the subsequent successful solution and refinement of the structure. The intensity data were collected using the $\theta/2\theta$ scan technique. A total of 5787 reflections were considered observed and were corrected for the effects of absorption. Full crystallographic details are given in Table S1.

The structure was solved using the Patterson interpretation routine of SHELXS-86[18] followed by tangent formula recycling, which revealed

Table 1. Crystallographic Data

empirical formula: $C_{37}H_{46}FeCl_4O_4N_4$	space group = *C2/c*
a = 27.454(7) Å	T = −150(2) °C
b = 15.322(3) Å	λ = 0.710 73 Å
c = 19.802(3) Å	ρ_{calcd} = 1.44 g cm^{-3}
β = 116.14(2)°	μ = 7.3 cm^{-1}
V = 7477.4 Å^3	$R_1(F_o)^a$ = 0.069
Z = 8	$R_2(F_o)^b$ = 0.063

^{a} $R_1 = \sum||F_o| - |F_c||/\sum|F_o|$. ^{b} $R_2 = [\sum w(|F_o| - |F_c|)^2/\sum wF_o^2]^{1/2}$.

(11) The 6−300 K magnetic susceptibility data for [Cu(OEP•)][SbCl$_6$] are cleanly fit by the Bleaney−Bowers model as a pair of weakly interacting Cu(II) ions with no residual magnetism attributable to the radical spins: Mondal, J. U.; Scheidt, W. R. Unpublished results.

(12) Brancato-Buentello, K.; Cheng, B.; Reddy, K. V.; Scheidt, W. R. Manuscript in preparation. We have also carried out spectroscopic studies measuring dimerization constants for a number of [M(OEP•)]$^+$ derivatives; K_{dim} for the copper complex is ∼100. There is no anion dependence for this complex with the perchlorate and hexachloroantimonate anions.[13]

(13) Brancato-Buentello, K. E.; Kang, S.-J.; Scheidt, W. R. Submitted for publication.

(14) Scheidt, W. R.; Song, H.; Haller, K. J.; Safo, M. K.; Orosz, R. D.; Reed, C. A.; Debrunner, P. G.; Schulz, C. E. *Inorg. Chem.* **1992**, *31*, 939.

(15) Adler, A. D.; Longo, F. R.; Kampas, F.; Kim, J. *J. Inorg. Nucl. Chem.* **1970**, *32*, 2443.

(16) Murata, Y.; Shine, H. J. *J. Org. Chem.* **1969**, *34*, 3368.

(17) Wolsey, W. C. *J. Chem. Educ.* **1973**, *50*, A335. *Chem. Eng. News* **1983**, *61* (Dec. 5), 4; **1963**, *41* (July 8), 47.

the positions of all 50 non-hydrogen atoms of the cation, anion, and solvate. All hydrogen atoms were located from difference electron density Fourier maps calculated after a preliminary least-squares refinement of the non-hydrogen atoms. The final cycles of refinement assigned anisotropic temperature factors to the non-hydrogen atoms and included the hydrogen atoms as fixed, idealized contributors (d_{C-H} = 0.95 Å, $B_H = 1.1 \times B_C$). The final data:variable ratio was 12.8:1. Refinement converged with unweighted and weighted agreement factors of $R_1 = 0.069$ and $R_2 = 0.063$; the estimated standard deviation of an observation of unit weight was 1.45. The final difference electron density Fourier map was judged free of significant features with the highest peak = 0.64 e/Å^3. Final atomic coordinates are listed in Table S2. Anisotropic thermal parameters for all non-hydrogen atoms and the fixed hydrogen atom coordinates are also available as Supporting Information (Tables S3 and S4).

Results

Small quantities of pure [Fe(OEP•)(Cl)]ClO_4 can be prepared by the hand selection of single crystals, and indeed, these crystals are of X-ray quality. However, bulk samples of [Fe(OEP•)(Cl)]ClO_4 (quantities large enough for Mössbauer and magnetic susceptibility studies) were always contaminated with [Fe(OEP•)$(OClO_3)_2$], presumably because of labile anions and differential solubilities. Although the low solubility of the [Fe(OEP•)(Cl)][$SbCl_6$] and [Fe(OEP•)(Br)][$SbCl_6$] derivatives prevented us from obtaining single-crystal specimens adequate for X-ray analysis, bulk samples of both hexachloroantimonate salts are readily prepared and are pure by Mössbauer criteria.

Mössbauer spectra of all species in a zero applied magnetic field display a single quadrupole doublet, except for that of [Fe(OEP•)(Cl)]ClO_4 which also shows a smaller, second doublet consistent with the presence of a small amount of [Fe(OEP•)-$(OClO_3)_2$]. The quadrupole doublets and isomer shifts at 4.2 K are ΔE_q =0.59 mm/s and $\delta = 0.41$ mm/s for [Fe(OEP•)(Cl)]-ClO_4, $\Delta E_q = 0.71$ mm/s and $\delta = 0.42$ mm/s for [Fe(OEP•)-(Cl)][$SbCl_6$], and $\Delta E_q = 0.77$ mm/s and $\delta = 0.41$ mm/s for [Fe(OEP•)(Br)][$SbCl_6$]. Mössbauer spectra of these radicals have also been obtained in a 4.5 T applied magnetic field. These spectra show a temperature-dependent magnetic broadening of the quadrupole doublet (Figure 1).

Temperature-dependent magnetic susceptibilities have been obtained from 2−300 K for [Fe(OEP•)(Cl)][$SbCl_6$] and 6−300 K for [Fe(OEP•)(Br)][$SbCl_6$]. Measurements were made at 2 and 10 kG. The lack of any field dependence confirmed that the samples were free of ferromagnetic impurities. Replicate measurements were made, and a Mössbauer spectrum was obtained on a portion of each sample. All samples showed only a single quadrupole doublet. Both species show similar temperature-dependent values for the magnetic moment. Data for [Fe(OEP•)(Br)][$SbCl_6$] are given in graphical form in Figure 2, and data for [Fe(OEP•)(Cl)][$SbCl_6$] are given in Figure 3. Data from Nakashima et al.[19] are also displayed in the top panel of Figure 3. Possible spin coupling models for the complexes were derived from consideration of both the magnetic susceptibility data and the Mössbauer data in an applied field. Complementary physical data are necessary in limiting the possible models.

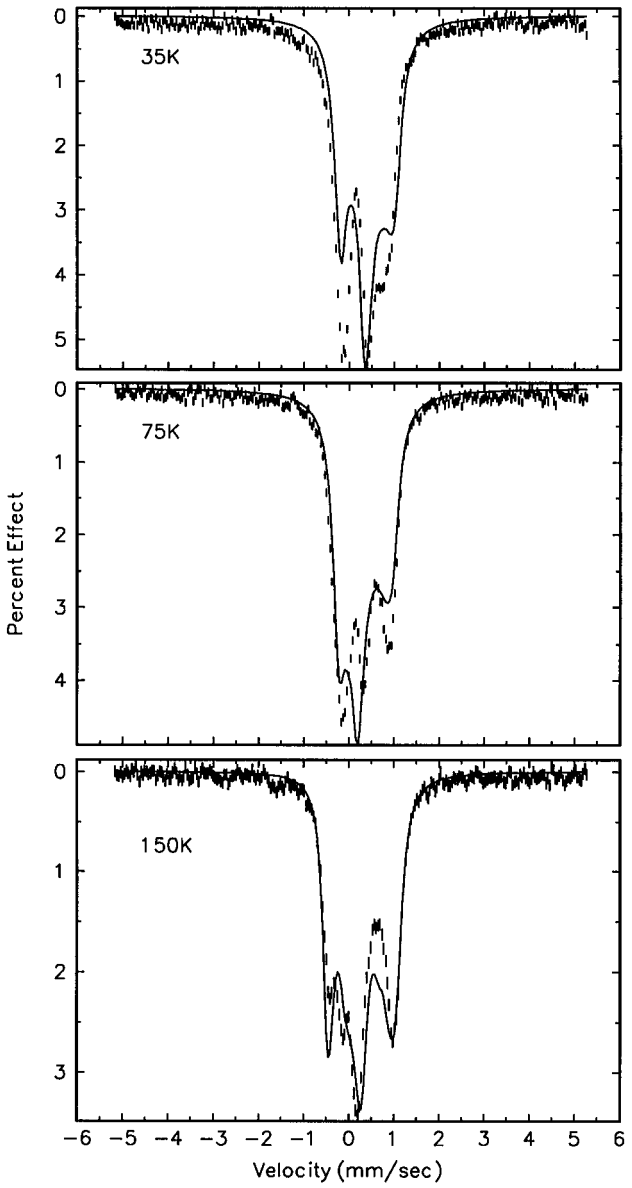

Figure 1. Mössbauer spectra of [Fe(OEP•)(Br)][$SbCl_6$] taken in an applied magnetic field of 45.6 kG parallel to the γ-ray direction at temperatures of 35, 75, and 150 K. The solid lines are simulations using the first model described in the text.

The molecular structure of the five-coordinate [Fe(OEP•)-(Cl)]$^+$ cation as the perchlorate salt is shown in Figure 4. The labeling scheme for the atoms employed in all tables is also shown in the diagram. Individual values of the bond distances and angles are given in Tables 2 and 3. The average value of the four Fe−N_p bonds is 2.058(5) Å, and the axial Fe−Cl bond distance is 2.186(1) Å. The displacement of the iron(III) atom out of the 24-atom mean plane is 0.43 and 0.46 Å from the N_4 plane. Figure 5 shows the displacements, in units of 0.01 Å, of the atoms of the 24-atom porphinato core from the best least-squares plane. The porphyrin core is slightly domed *toward* the iron atom, i.e., the core exhibits a rather unusual reverse doming. Nonetheless, all deviations from exact planarity are less than 0.08 Å. [Fe(OEP•)(Cl)]$^+$ cations exist as cofacial dimers in the solid state. Two orthogonal views of the cofacial $\pi-\pi$ dimer are given in Figures 6 and 7. The two iron(III) atoms in the dimer are separated by 4.112(1) Å, the Ct···Ct

(18) Sheldrick, G. *Acta Crystallogr., Sect. A* **1990**, *A46*, 467. Other programs used in this study included local modifications of Jacobson's ALLS, Zalkin's FORDAP, Busing and Levy's ORFFE and ORFLS, the SDP package of Enraf-Nonius, and Johnson's ORTEP2. Atomic form factors were from: Cromer, D. T.; Mann, J. B. *Acta Crystallogr., Sect. A* **1968**, *A24*, 321. Real and imaginary corrections for anomalous dispersion in the form factor of the iron and chlorine atoms were from: Cromer, D. T.; Liberman, D. J. *J. Chem. Phys.* **1970**, *53*, 1891. Scattering factors for hydrogen were from: Stewart, R. F.; Davidson, E. R.; Simpson, W. T. *J. Chem. Phys.* **1965**, *42*, 3175. All calculations were performed on VAXstation 3200 and 4000-90 computers.

(19) Nakashima, S.; Ohya-Nishiguchi, H.; Hirota, N.; Fujii, H.; Morishima, I. *Inorg. Chem.* **1990**, *29*, 5207.

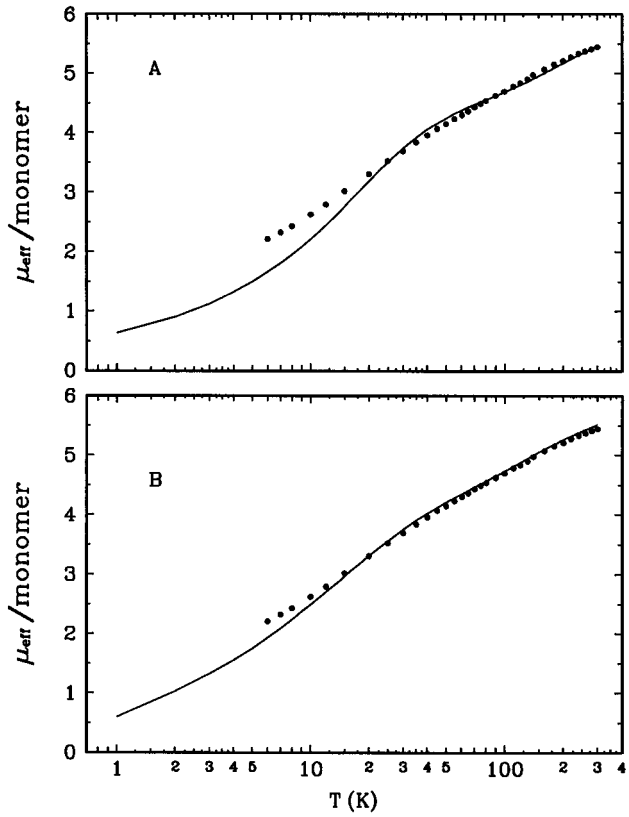

Figure 2. Magnetic susceptibility data for [Fe(OEP•)(Br)][$SbCl_6$] in an applied field of 10 kG. The experimental data are shown as filled circles, while the solid lines are calculated using multiparameter spin coupling models. Panel A shows the fit with the spin coupling model in which there is intermolecular coupling of the total spins and using parameters given in the text. Panel B shows the fit with the second model described in the text with three spin coupling (*J*) parameters.

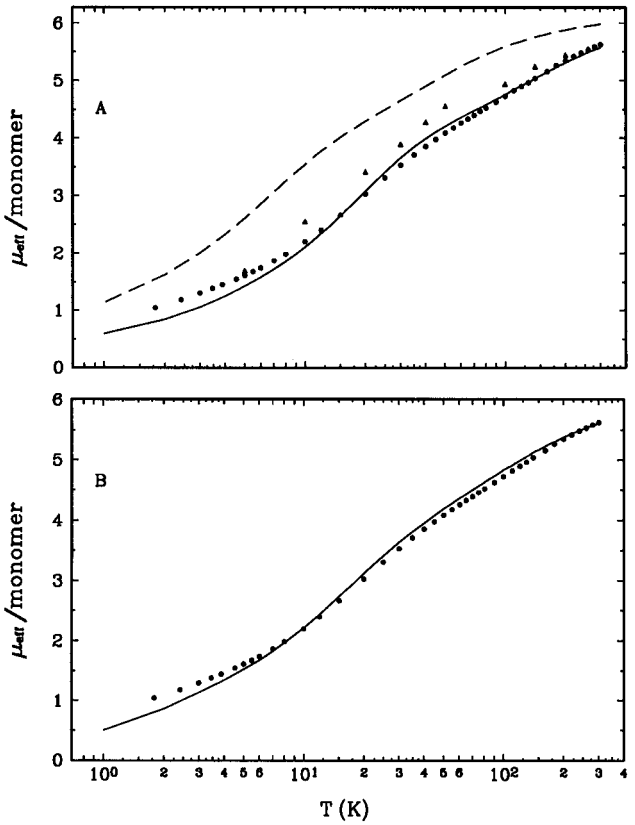

Figure 3. Magnetic susceptibility data for [Fe(OEP•)(Cl)][$SbCl_6$] in an applied field of 10 kG. The experimental data are shown as filled circles, while the solid lines are calculated using multiparameter spin coupling models. Panel A shows the fit with the spin coupling model in which there is intermolecular coupling of the total spins and using parameters given in the text. Panel B shows the fit with the second model described in the text with three spin coupling (*J*) parameters. Panel A also shows the data reported by Nakashima et al.[19] (filled triangles). The dashed line is the fit to the data using the parameters presented by Nakashima et al.[19]

separation is 3.25 Å, the separation between the two mean planes is 3.24 Å, and the lateral shift is 0.2 Å.

Discussion

The coordination geometry of the five-coordinate [Fe(OEP•)(Cl)]$^+$ cation, as the perchlorate salt, is that expected for a high-spin iron(III) porphyrinate derivative: a square pyramidal FeN_4X group with values for the Fe−N_p and Fe−X bonds and the iron atom displacement within the range of previously observed values.[20] Thus, in agreement with earlier observations, the formation of a porphyrin π-cation radical seems to have a minimal effect on the metal ion coordination geometry. Furthermore, physical properties that probe the spin state, notably Mössbauer spectroscopy, also unambiguously lead to an assignment of a high-spin state to the iron. Thus, all attempts to describe the electronic structure and magnetic properties of these species should utilize an $S = {}^5/_2$ state for iron(III).

As we have observed for other four- and five-coordinate [M(OEP•)]$^+$ radicals, the cation of [Fe(OEP•)(Cl)]ClO_4 forms a solid-state cofacial dimer in which the two porphyrin rings interact quite strongly. There are two previously structurally characterized species of this type, the [Zn(OEP•)(OH_2)]$^+$ and [Ni(OEP•)]$^+$ cations.[5] Both also form cofacial dimers, and we believe that such solid-state dimer formation is a very general phenomenon for OEP π-cation radicals. Figure 6 shows that two porphyrin planes in the [Fe(OEP•)(Cl)]$_2^{2+}$ dimer approach each other closely; the interplanar separation between the two least-squares planes is found to be a strikingly small 3.24 Å.

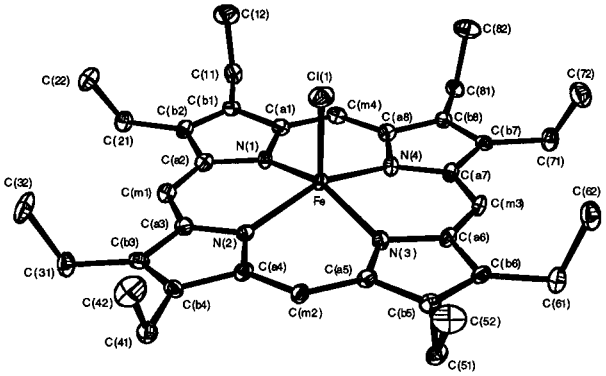

Figure 4. ORTEP diagram of the [Fe(OEP•)(Cl)]$^+$ π-cation radical showing the atom labeling scheme. Thermal ellipsoids of all atoms are contoured at the 50% probability level. Hydrogen atoms have been omitted for clarity.

Corresponding values in [Zn(OEP•)(OH_2)]$^+$ and [Ni(OEP•)]$^+$ are 3.31 and 3.19 Å, respectively. In all cases, the interplanar separation is smaller than that of the ∼3.35 Å spacing of graphite; moreover, the C···C separations in the radicals are much smaller than those in graphite. Although not required by the crystallographic symmetry, the two porphyrin planes are parallel to each other within 0.2°. (The two planes of Figures 6 and 7 are related by a crystallographic 2-fold axis.)

The perpendicular view of the cofacial dimer (Figure 7) shows that the two rings are directly above each other (i.e., the lateral shift is effectively zero). Such completely overlapped rings are

(20) Scheidt, W. R.; Reed, C. A. *Chem. Rev.* **1981**, *81*, 543.

Table 2. Bond Distances (Å) in $[Fe(OEP^{\bullet})(Cl)]ClO_4$[a]

Fe−Cl(1)	2.186(1)	C(a8)−C(m4)	1.373(5)
Fe−N(1)	2.055(3)	C(b1)−C(b2)	1.355(5)
Fe−N(2)	2.063(3)	C(b3)−C(b4)	1.346(5)
Fe−N(3)	2.052(3)	C(b5)−C(b6)	1.356(5)
Fe−N(4)	2.062(3)	C(b7)−C(b8)	1.355(5)
N(1)−C(a1)	1.364(4)	C(b1)−C(11)	1.487(5)
N(1)−C(a2)	1.384(5)	C(b2)−C(21)	1.501(5)
N(2)−C(a3)	1.357(5)	C(b3)−C(31)	1.502(5)
N(2)−C(a4)	1.386(4)	C(b4)−C(41)	1.504(5)
N(3)−C(a5)	1.356(4)	C(b5)−C(51)	1.500(5)
N(3)−C(a6)	1.398(5)	C(b6)−C(61)	1.490(5)
N(4)−C(a7)	1.350(5)	C(b7)−C(71)	1.505(5)
N(4)−C(a8)	1.394(4)	C(b8)−C(81)	1.499(5)
C(a1)−C(b1)	1.461(5)	C(11)−C(12)	1.519(5)
C(a1)−C(m4)	1.402(5)	C(21)−C(22)	1.534(6)
C(a2)−C(b2)	1.459(5)	C(31)−C(32)	1.530(6)
C(a2)−C(m1)	1.371(5)	C(41)−C(42)	1.528(6)
C(a3)−C(b3)	1.450(5)	C(51)−C(52)	1.525(5)
C(a3)−C(m1)	1.403(5)	C(61)−C(62)	1.550(6)
C(a4)−C(b4)	1.457(5)	C(71)−C(72)	1.525(6)
C(a4)−C(m2)	1.372(5)	C(81)−C(82)	1.524(5)
C(a5)−C(b5)	1.456(5)	C1(2)−O(1)	1.449(3)
C(a5)−C(m2)	1.408(5)	C1(2)−O(2)	1.439(3)
C(a6)−C(b6)	1.452(5)	C1(2)−O(3)	1.447(3)
C(a6)−C(m3)	1.371(5)	C1(2)−O(4)	1.439(3)
C(a7)−C(b7)	1.439(5)	C(9)−C1(3)	1.758(4)
C(a7)−C(m3)	1.410(5)	C(9)−C1(4)	1.767(4)
C(a8)−C(b8)	1.450(5)	Fe−Fe′[b]	4.112(1)

[a] Estimated standard deviations in the least significant digits are given in parentheses. [b] Coordinates of primed atoms are related to those of the corresponding unprimed atoms by the transformation $1 - x, y, 0.5 - z$.

found in both of the previously characterized OEP cation radicals, but are otherwise unknown in porphyrin structures. It is interesting to note that the unusual reverse doming of the core in $[Fe(OEP^{\bullet})(Cl)]ClO_4$ leads to slightly closer inter-ring contacts than would be the case for a more planar species, suggesting the probable stabilizing effects of the inter-ring contacts. Moreover, bond distances in the inner 16-membered ring show a quite unusual alternating pattern that must result from a strong inter-ring interaction (vide infra). The great inner 16-membered ring consists of eight $N-C_a$ and eight C_a-C_m bonds which, in metalloporphyrins, are invariably equivalent and are consistent with a completely delocalized system. In the present case, however, the $N-C_a$ and C_a-C_m bonds divide into alternating "long" and "short" sets. The pattern and individual values of the bond distances are shown in Figure 5. Average values are 1.357(6) or 1.391(7) Å for $N-C_a$ bonds, and average C_a-C_m bond distances are 1.372(1) or 1.406(4) Å. The number in parentheses following each averaged value is the estimated standard deviation calculated on the assumption that the averaged values are drawn from the same population; the differences in the sets are clearly statistically significant. Further evidence for the experimental significance of the differences in these sets is given by the close agreement in all values for the C_a-C_b and C_b-C_b bond distances: average values are 1.453(7) and 1.353(5) Å, respectively.

A similar alternating bond distance pattern has been observed for the zinc radical dimer but not for the nickel radical dimer and naturally leads to the question of the basis for the effect. A comparison of the inter-ring geometry and concomitant inter-ring interactions in $[Fe(OEP^{\bullet})(Cl)]ClO_4$ with the previously characterized radical dimers is especially revealing. The relative orientation of the two rings of the dimer (twist angle), as measured by the average N−Fe−Fe′−N′ dihedral angle, is 31.2°. The value in the Zn derivative is virtually identical at 31.3°, while the Ni complex has a twist angle of 40.4°. The differences in twist angles leads to differing, close C···C inter-

Table 3. Bond Angles (deg) in $[Fe(OEP^{\bullet})(Cl)]ClO_4$

Cl(1)−Fe−N(1)	103.10(9)	C(a1)−C(b1)−C(11)	125.6(3)
Cl(1)−Fe−N(2)	104.47(9)	C(b2)−C(b1)−C(11)	128.1(3)
Cl(1)−Fe−N(3)	102.29(9)	C(a2)−C(b2)−C(b1)	106.9(3)
Cl(1)−Fe−N(4)	101.20(9)	C(a2)−C(b2)−C(21)	123.7(3)
N(1)−Fe−N(2)	87.5(1)	C(b1)−C(b2)−C(21)	129.4(3)
N(1)−Fe−N(3)	154.6(1)	C(a3)−C(b3)−C(b4)	106.7(3)
N(1)−Fe−N(4)	87.0(1)	C(a3)−C(b3)−C(31)	124.9(3)
N(2)−Fe−N(3)	86.6(1)	C(b4)−C(b3)−C(31)	128.4(3)
N(2)−Fe−N(4)	154.3(1)	C(a4)−C(b4)−C(b3)	106.6(3)
N(3)−Fe−N(4)	87.6(1)	C(a4)−C(b4)−C(41)	125.3(3)
Fe−N(1)−C(a1)	126.1(2)	C(b3)−C(b4)−C(41)	128.1(3)
Fe−N(1)−C(a2)	125.8(2)	C(a5)−C(b5)−C(b6)	107.0(3)
C(a1)−N(1)−C(a2)	105.5(3)	C(a5)−C(b5)−C(51)	125.8(3)
Fe−N(2)−C(a3)	126.7(2)	C(b6)−C(b5)−C(51)	127.2(3)
Fe−N(2)−C(a4)	126.2(2)	C(a6)−C(b6)−C(b5)	106.2(3)
C(a3)−N(2)−C(a4)	105.2(3)	C(a6)−C(b6)−C(61)	123.9(3)
Fe−N(3)−C(a5)	127.0(2)	C(b5)−C(b6)−C(61)	129.8(3)
Fe−N(3)−C(a6)	125.2(2)	C(a7)−C(b7)−C(b8)	106.3(3)
C(a5)−N(3)−C(a6)	105.2(3)	C(a7)−C(b7)−C(71)	125.0(3)
Fe−N(4)−C(a7)	126.3(2)	C(b8)−C(b7)−C(71)	128.7(3)
Fe−N(4)−C(a8)	125.7(2)	C(a8)−C(b8)−C(b7)	106.8(3)
C(a7)−N(4)−C(a8)	105.0(3)	C(a8)−C(b8)−C(81)	126.0(3)
N(1)−C(a1)−C(b1)	111.1(3)	C(b7)−C(b8)−C(81)	127.2(3)
N(1)−C(a1)−C(m4)	124.5(3)	C(a2)−C(m1)−C(a3)	125.7(4)
C(b1)−C(a1)−C(m4)	124.3(3)	C(a4)−C(m2)−C(a5)	125.8(3)
N(1)−C(a2)−C(b2)	110.2(3)	C(a6)−C(m3)−C(a7)	126.4(3)
N(1)−C(a2)−C(m1)	125.3(3)	C(a1)−C(m4)−C(a8)	126.1(3)
C(b2)−C(a2)−C(m1)	124.5(4)	C(b1)−C(11)−C(12)	113.3(3)
N(2)−C(a3)−C(b3)	111.3(3)	C(b2)−C(21)−C(22)	113.3(3)
N(2)−C(a3)−C(m1)	124.9(3)	C(b3)−C(31)−C(32)	114.0(3)
C(b3)−C(a3)−C(m1)	123.7(3)	C(b4)−C(41)−C(42)	113.3(3)
N(2)−C(a4)−C(b4)	110.1(3)	C(b5)−C(51)−C(52)	112.8(3)
N(2)−C(a4)−C(m2)	124.3(3)	C(b6)−C(61)−C(62)	112.0(3)
C(b4)−C(a4)−C(m2)	125.6(3)	C(b7)−C(71)−C(72)	113.3(3)
N(3)−C(a5)−C(b5)	111.1(3)	C(b8)−C(81)−C(82)	112.6(3)
N(3)−C(a5)−C(m2)	124.6(3)	O(1)−Cl(2)−O(2)	109.5(2)
C(b5)−C(a5)−C(m2)	124.3(3)	O(1)−Cl(2)−O(3)	109.3(2)
N(3)−C(a6)−C(b6)	110.4(3)	O(1)−Cl(2)−O(4)	109.5(2)
N(3)−C(a6)−C(m3)	124.6(3)	O(2)−Cl(2)−O(3)	109.4(2)
C(b6)−C(a6)−C(m3)	125.0(3)	O(2)−Cl(2)−O(4)	109.7(2)
N(4)−C(a7)−C(b7)	112.1(3)	O(3)−Cl(2)−O(4)	109.5(2)
N(4)−C(a7)−C(m3)	124.3(3)	Cl(3)−C(9)−Cl(4)	111.7(2)
C(b7)−C(a7)−C(m3)	123.6(3)	Fe′−Fe−Cl(1)	176.53(4)
N(4)−C(a8)−C(b8)	109.8(3)	Fe′−Fe−N(1)	77.14(9)
N(4)−C(a8)−C(m4)	124.4(3)	Fe′−Fe−N(2)	78.99(9)
C(b8)−C(a8)−C(m4)	125.8(3)	Fe′−Fe−N(3)	77.49(9)
C(a1)−C(b1)−C(b2)	106.2(3)	Fe′−Fe−N(4)	75.33(9)

ring contacts. Magnetic data for all of the OEP dimers are consistent with strong inter-ring coupling, but this does not lead to the formation of a carbon−carbon bond as has been recently observed[21] for a (octaethyloxophlorin radical) nickel(II) derivative. In the nickel complex, the inter-ring interaction pattern is a simple 8-fold set of $C_a\cdots C_a$ interactions. If the inter-ring interaction is between π-cation ring atoms with the highest unpaired electron density, this $C_a\cdots C_a$ is precisely the pattern expected for the interaction of a pair of a_{1u} radical cations. However, the iron and zinc species have a different inter-ring orientation, one in which the close contacts are between the C_a and C_m atoms in the pattern $C_a\cdots C_a$, $C_a\cdots C_m$, $C_m\cdots C_a$, etc., around the inner 16-membered ring (cf. Figure 7).[22]

The small Mössbauer quadrupole splitting constants for the two $[Fe(OEP^{\bullet})(Cl)]^+$ derivatives and for $[Fe(OEP^{\bullet})(Br)][SbCl_6]$ clearly indicate that the iron centers are high spin. The isomer shift values require the assignment of a +3 oxidation state,

(21) Balch, A. L.; Noll, B. C.; Reid, S. M.; Zovinka, E. P. *J. Am. Chem. Soc.* **1993**, *115*, 2431.

(22) Czernuszewicz et al. (Czernuszewicz, R.; Macor, K. A.; Li, X.-Y.; Kincaid, J. R.; Spiro, T. G. *J. Am. Chem. Soc.* **1995**, *111*, 3860) have suggested that owing to the near-degeneracy of the A_{1u} and A_{2u} ground states, a pseudo-Jahn−Teller effect should arise and could lead to bond alternation. We are continuing our studies on this interesting bond alternation effect.

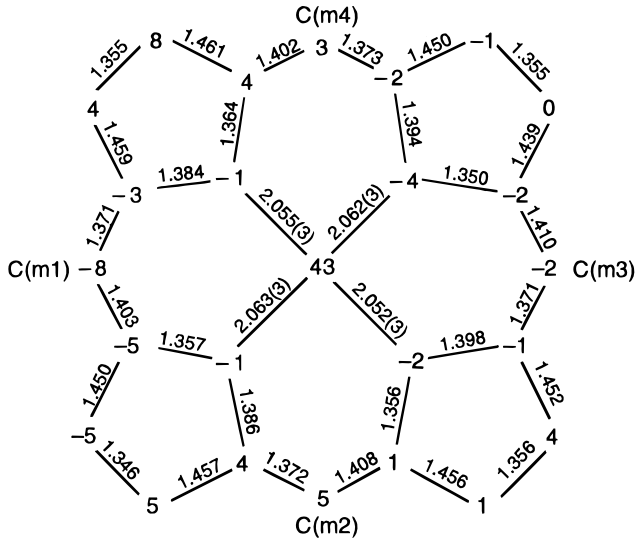

Figure 5. Formal diagram of the porphinato core displaying perpendicular displacements, in units of 0.01 Å, of the core atoms from the 24-atom mean plane. Also entered on the diagram are the values of the individual bond distances in the core and coordination group. Note the alternating short−long pattern of the N−C_a and C_a−C_m bond distances in the great inner 16-membered ring.

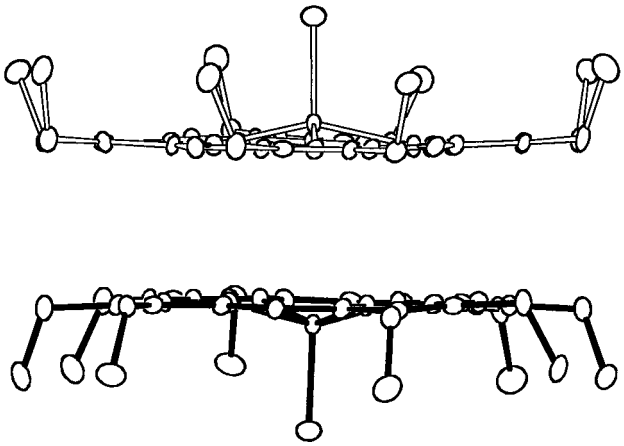

Figure 6. An edge-on ORTEP diagram of the cofacial dimer formed by two [Fe(OEP•)(Cl)]+ π-cation radicals. The horizontal axis is parallel to and the vertical axis is perpendicular to the 24-atom mean plane. Atoms are contoured at the 50% probability level.

thereby further confirming the π-cation radical assignment. Most importantly, the fact that the Mössbauer spectra are not split by the presence of a weak magnetic field strongly suggests that iron(III) must be coupled to other spins so that the systems no longer have half-integer spins. This latter point places definite restrictions on spin−spin coupling models that can be used to fit the magnetic susceptibility data. However, analysis of the data is complicated by the effects of intermediate spin fluctuation rates at temperatures below 35 K, even in a large applied field. We were able to get good fits to the data above 35 K using the ω-tensor model of Kent et al.[23] The ω-tensor components are temperature dependent and should be proportional to the thermal-averaged spin expectation values for the iron spin. Knowledge of the ω-tensor components and the spin expectation values allows one to calculate the components of the magnetic hyperfine tensor **A** of the iron.

The magnetic susceptibility data for $[Fe(OEP^{\bullet})(Br)]_2[SbCl_6]_2$ are shown in Figure 2; $[Fe(OEP^{\bullet})(Cl)]_2[SbCl_6]_2$ shows a quite

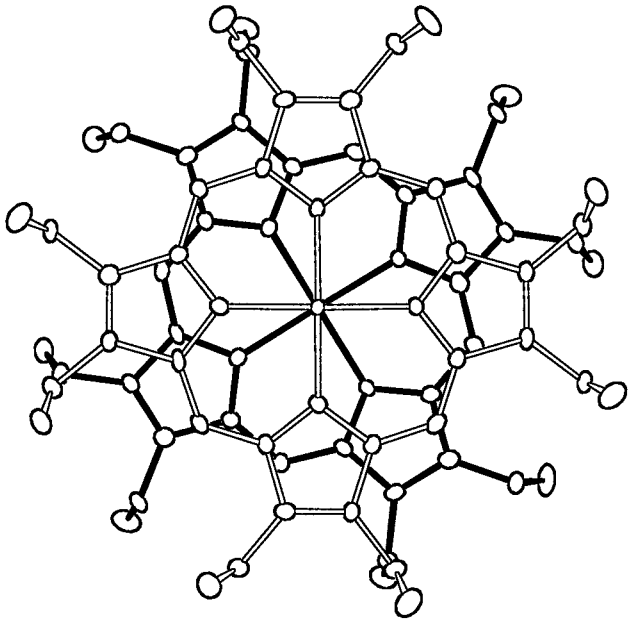

Figure 7. ORTEP diagram of the cofacial dimer showing the overlap between the two porphyrin rings. The least-squares porphyrin plane is parallel to the plane of the paper. The axial chloride ligand has not been drawn.

similar temperature dependence. We have been able to produce acceptable fits to the data for the bromide and chloride complexes with two models that treat the coupling between the spins somewhat differently. The first model is that which we described previously[14] for $[Fe(OEP^{\bullet})(Cl)]_2[SbCl_6]_2$ and which had been developed by Lang et al.[24] for $[Fe(TPP^{\bullet})(Cl)][SbCl_6]$. In this model, there are three terms in the total Hamiltonian: an axial zero-field splitting parameter D for the high-spin iron, an intramolecular magnetic coupling $-2J_{Fe-r}(\vec{S}\cdot\vec{s})$ between the iron spin $S = {}^5/_2$ and the π-cation radical $s = {}^1/_2$ spin, and an intermolecular coupling $-2J_{R-R}(\vec{S} + \vec{s})\cdot(\vec{S}' + \vec{s}')$ between the total spins on each half of the dimer. The second model uses a Hamiltonian with D and $-2J_{Fe-r}(\vec{S}\cdot\vec{s})$, as before, along with additional coupling of the spins of the two radicals, $-2J_{r-r}(\vec{s}\cdot\vec{s}')$, and the interaction between the two iron atoms, $-2J_{Fe-Fe}(\vec{S}\cdot\vec{S}')$.

The magnetic susceptibility data do not allow us to distinguish between the two coupling models. With the first coupling model there is a range of parameters that gives acceptable fits to the susceptibility data. Two such sets for $[Fe(OEP^{\bullet})(Br)]_2[SbCl_6]_2$ are $D = 35$ cm^{-1}, $2J_{Fe-r} = -83$ cm^{-1}, and $2J_{R-R} = -3$cm^{-1} or $D = 10$ cm^{-1}, $2J_{Fe-r} = -83$ cm^{-1}, and $2J_{R-R} = -4$ cm^{-1}. Since the calculated iron spin expectation values are quite different for these two parameter sets, they will produce different components of the hyperfine tensor, as calculated using the Mössbauer-determined ω-tensor. For the set with $D = 35$ cm^{-1}, the tensor components are $A_{xx} = A_{yy} = -21Tg_n\beta_n$, and $A_{zz} = -40Tg_n\beta_n$, while for the set with $D = 10$ cm^{-1}, the components are $A_{xx} = A_{yy} = A_{zz} = -18Tg_n\beta_n$. Since the high-spin ferric **A** tensor is expected to be nearly isotropic, we conclude that the parameter set with the smaller zero-field splitting constant is the more reasonable one. It is also to be noted that this value of D is comparable to values of D measured for other high-spin iron(III) porphyrinates.[25] Applying the same Mössbauer and susceptibility fit criteria to the data for $[Fe(OEP^{\bullet})(Cl)]_2[SbCl_6]_2$, we obtain $D = 10$ cm^{-1}, $2J_{Fe-r} = -63$ cm^{-1}, $2J_{R-R}$

(23) Kent, T. A.; Spartalian, K.; Lang, G.; Yonetani, T. *Biochem. Biophys. Acta* **1977**, *490*, 331.

(24) Lang, G.; Boso, B.; Erler, B. S.; Reed, C. A. *J. Chem. Phys.* **1986**, *84*, 2998.

(25) Debrunner, P. G. In *Iron Porphyrins, Part III*; Lever, A. B. P., Gray, H. B., Eds.; VCH: New York, 1989; pp 139−227.

$= -4$ cm^{-1}, $A_{xx} = A_{yy} = -24Tg_n\beta_n$, and $A_{zz} = -25Tg_n\beta_n$. The value of D is now smaller than in our previous fit[14] and is now more consistent with the value expected for iron(III). A comparison of the chloro and bromo complex values shows that the antiferromagnetic iron−radical coupling is slightly weaker in the chloro complex, while the intermolecular magnetic coupling is about the same. Most significantly, the chloro and bromo complexes have quite similar values that fit both the measured magnetic susceptibilities and Mössbauer parameters.

The second model also leads to acceptable calculated fits for the magnetic susceptibility and the magnetic Mössbauer data for both the chloride and bromide complexes. The values obtained for $[Fe(OEP^{\bullet})(Br)]_2[SbCl_6]_2$ are $2J_{r-r} = -348$ cm^{-1}, $2J_{Fe-r} = -118$ cm^{-1}, $2J_{Fe-Fe} = 3$ cm^{-1} and D = 1 cm^{-1}, $A_{xx} = A_{yy} = -24Tg_n\beta_n$, and $A_{zz} = -16Tg_n\beta_n$. The values determined for $[Fe(OEP^{\bullet})(Cl)]_2[SbCl_6]_2$ are $2J_{r-r} = -278$ cm^{-1}, $2J_{Fe-r} = -90$ cm^{-1}, $2J_{Fe-Fe} = 1$cm^{-1} and D = 3 cm^{-1}, $A_{xx} = A_{yy} = -24Tg_n\beta_n$, and $A_{zz} = -22Tg_n\beta_n$. This model explicitly shows the strong coupling between the two porphyrin radicals in the dimer, in agreement with other derivatives. However, the calculated value of D appears to be unrealistically low for an iron(III) complex. When the value of D is increased to reasonable values in this model, there is a significant disparity in the fit of the very low temperature susceptibility data ($T <$ 20 K) for all J values.

The first model thus gives better fits to the magnetic data when the additional requirement of a physically meaningful value of D is included. This model also yields a qualitatively correct result for the temperature variation of the magnetic hyperfine splitting in the Mössbauer spectra. The solid lines in Figure 1 are simulations of the $[Fe(OEP^{\bullet})(Br)][SbCl_6]$ spectra using the electronic parameters that fit the susceptibility data for the first model, assuming that the fast spin fluctuation approximation is valid. In these simulations, we varied only the parameters A_{xx} ($=A_{yy}$) and A_{zz} to match the experimental data. The resulting hyperfine tensor, $A_{xx} = A_{yy} = 18.4Tg_n\beta_n$ and $A_{zz} = 18.8Tg_n\beta_n$, is a very reasonable result for high-spin Fe(III). We note that the simulation best matches the data at the higher temperatures and conclude that a dynamic model which allows intermediate spin fluctuation rates would be necessary to accurately reproduce the details of the Mössbauer spectra.

At first glance, it might seem surprising that the second model, with its three coupling constants, should not fit the susceptibility data better than the first model, with its two coupling constants. However, the total spin formulation of the first model implicitly includes contributions from all possible couplings between the four different spin centers of the dimer.

It is to be noted that both coupling models lead to a picture of an antiferromagnetically coupled porphyrin radical and a high-spin iron(III) in the $[Fe(OEP^{\bullet})(X)]^+$ systems. Given the effective planarity of the porphinato core, it might have been thought that the iron(III) and radical spins should display ferromagnetic coupling.[7] However, unlike $[Cu(TMP^{\bullet})]^+$ [4] or $[Fe(TPP^{\bullet})(OClO_3)_2]$,[1] the metal atom is substantially out of the porphyrin plane. The effective local symmetry of five-coordinate $[Fe(OEP^{\bullet})(X)]^+$ can be no higher than C_{4v}, rather than D_{4h}. In this symmetry (and any possible lower symmetry), the porphyrin a_{1u} orbital and the iron d_{z^2} orbital are not strictly orthogonal. There will be net overlap, and thus, antiferromagnetic coupling is allowed. It is important to note that for this system, the planarity or nonplanarity of the porphyrin macrocycle is unimportant. Lastly, we note that the magnitude of the coupling between the nominal a_{1u} radical[26] and Fe(III) in $[Fe(OEP^{\bullet})(X)]^+$ ($|2J| \sim 100$ cm^{-1}) is larger than might be expected.[7,25,27] More data on a_{1u} vs a_{2u} comparisons are necessary, however, before any conclusions can be reached.

Summary

We have reported the molecular structure of the π-cation radical complex $[Fe(OEP^{\bullet})(Cl)]ClO_4$ and complete magnetic susceptibility and Mössbauer studies on two related species $[Fe(OEP^{\bullet})(Cl)][SbCl_6]$ and $[Fe(OEP^{\bullet})(Br)][SbCl_6]$. The structural analysis shows that $[Fe(OEP^{\bullet})(Cl)]ClO_4$ exists as a dimer in the crystalline state, and this was also assumed in the analysis of the magnetic properties of the related hexachloroantimonate salts. All data are consistent with the presence of high-spin iron(III) centers strongly coupled to the porphyrin radical with additional interaction between the pair of rings in the solid-state dimers.

Acknowledgment. We acknowledge, with thanks, the support of the National Institutes of Health under Grants GM-38401 (W.R.S.), GM-23851 (C.A.R.), GM-16406 (P.G.D.), and GM-48513 (C.E.S.).

Supporting Information Available: Tables of crystal data and intensity collection parameters, fractional coordinates, atomic displacement parameters, and fixed hydrogen coordinates for $[Fe(OEP)Cl]ClO_4 \cdot CH_2Cl_2$ (5 pages) and an X-ray crystallographic file, in CIF format, is available. Access and/or ordering information is given on any current masthead page.

IC961053D

(26) An a_{1u} radical assignment is made by comparison to other OEP radical cations; the ground state is primarily the result of the peripheral substiutents.

(27) (a) Fujii, H.; Yoshimura, T.; Kamada, H. *Inorg. Chem.* **1996**, *35*, 2373. (b) Jayaraj, K.; Terner, J.; Gold, A.; Roberts, D. A.; Austin, R. N.; Mandon, D.; Weiss, R.; Bill, E.; Müther, M.; Trautwein, A. X. *Inorg. Chem.* **1996**, *35*, 1632 and references therein.